

Quantum phase transitions driven by rhombic-type single-ion anisotropy in the $S=1$ Haldane chain

Yu-Chin Tzeng (曾郁欽),^{1,2,*} Hiroaki Onishi (大西弘明),^{3,†}
 Tsuyoshi Okubo (大久保毅),⁴ and Ying-Jer Kao (高英哲)^{2,5,‡}

¹Department of Physics, National Chung-Hsing University, Taichung 40227, Taiwan

²Department of Physics, National Taiwan University, Taipei 10617, Taiwan

³Advanced Science Research Center, Japan Atomic Energy Agency, Tokai, Ibaraki 319-1195, Japan

⁴Department of Physics, University of Tokyo, Tokyo 113-0033, Japan

⁵National Center of Theoretical Sciences, National Tsing Hua University, Hsinchu 300, Taiwan

(Dated: November 11, 2018)

The spin-1 Haldane chain is an example of the symmetry-protected-topological (SPT) phase in one dimension. Experimental realization of the spin chain materials usually involves both the uniaxial-type, $D(S^z)^2$, and the rhombic-type, $E[(S^x)^2 - (S^y)^2]$, single-ion anisotropies. Here, we provide a precise ground-state phase diagram for spin-1 Haldane chain with these single-ion anisotropies. Using quantum numbers, we find that the \mathbb{Z}_2 symmetry breaking phase can be characterized by double degeneracy in the entanglement spectrum. Topological quantum phase transitions take place on particular paths in the phase diagram, from the Haldane phase to the Large- E_x , Large- E_y , or Large- D phases. The topological critical points are determined by the level spectroscopy method with a newly developed parity technique in the density-matrix renormalization group [Phys. Rev. B **86**, 024403 (2012)], and the Haldane-Large- D critical point is obtained with an unprecedentedly precision, $(D/J)_c=0.9684713(1)$. Close to this critical point, a small rhombic single-ion anisotropy $|E|/J \ll 1$ can destroy the Haldane phase and bring the system into a y -Néel phase. We propose that the compound $[\text{Ni}(\text{HF}_2)(3\text{-Clpy})_4]\text{BF}_4$ is a candidate system to search for the y -Néel phase.

PACS numbers: 75.10.Pq

Introduction.— Quantum magnetism of integer-spin chains has been attracting attention for decades. It was stimulated by the Haldane conjecture [1] that the lowest excitation in the antiferromagnetic Heisenberg model are gapped if and only if the spin S is an integer. Experimental evidences for the Haldane gap were discovered in several $S=1$ quasi-one dimensional (Q1D) materials, *e.g.*, CsNiCl_3 [2, 3], Y_2BaNiO_5 [4–6], $\text{Ni}(\text{C}_2\text{H}_8\text{N}_2)_2\text{NO}_2(\text{ClO}_4)$ (NENP) [7, 8] and $[\text{Ni}(\text{C}_2\text{H}_8\text{N}_2)_2\text{NO}_2]\text{BF}_4$ (NENB) [9]. Due to the crystal field, the microscopic effective Hamiltonian for the Q1D spin chains involves the single-ion anisotropies,

$$H = J \sum_{i=1}^L \vec{S}_i \cdot \vec{S}_{i+1} + D \sum_{i=1}^L (S_i^z)^2 + E \sum_{i=1}^L [(S_i^x)^2 - (S_i^y)^2], \quad (1)$$

where $J > 0$ is the strength of the Heisenberg exchange interaction, as well as D and E are the parameters of the uniaxial and rhombic single-ion anisotropies, respectively. The Haldane gap is robust against small anisotropies, and it extends to a region so-called Haldane phase. In the absence of a local order, the Haldane phase falls beyond the paradigm of Landau’s theory of phase transitions. From a topological point of view, the Haldane phase is classified as the symmetry-protected-topological (SPT) phase [10] for odd- S , while the Haldane phase is adiabatically connected with a topological trivial phase for even- S [11–15]. Interesting properties such as the Valence-Bond-Solid (VBS) description [16], hidden $\mathbb{Z}_2 \times \mathbb{Z}_2$ symmetry breaking, non-local string or-

der, fractionalized gapless edge modes, and the degenerate entanglement spectra are used to characterize the SPT phase. On the other hand, the entanglement spectrum is not required to be degenerate for both the topological trivial phase and the symmetry breaking phase.

Prior theoretical and numerical investigations focus on the effects of the uniaxial anisotropy (D -term) [17–24]. The effect of rhombic anisotropy (E -term) lacks a com-

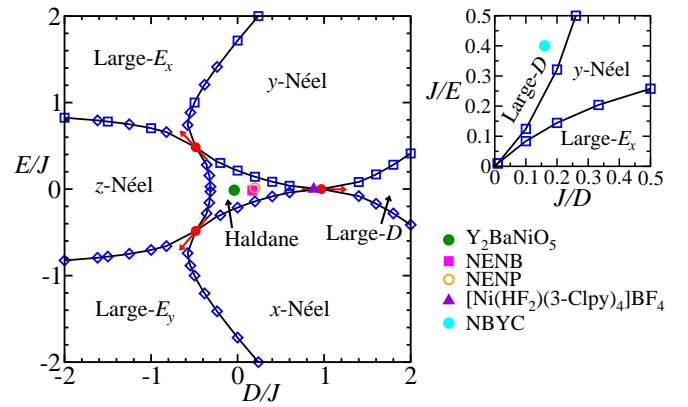


FIG. 1. Quantum phase diagram for $S=1$ Haldane chain with both uniaxial and rhombic single-ion anisotropies. Topological quantum phase transitions occur through particular (red arrows) routes. The Haldane-Large- D critical point $(D/J)_c=0.9684713(1)$ is determined by the LS+DMRG method. A small rhombic anisotropy $|E|/J \ll 1$ at this point $(D/J)_c$ induces a transverse antiferromagnetic order.

plete theoretical understanding [25, 26]; however, materials with large D/J and E/J are discovered, *e.g.*, the $S=1$ Q1D chains, $\text{Sr}_3\text{NiPtO}_6$ [27, 28], $\text{Ni}(\text{C}_2\text{H}_8\text{N}_2)_2\text{Ni}(\text{CN})_4$ (NENC) [29], $[\text{Ni}(\text{HF}_2)(3\text{-Clpy})_4]\text{BF}_4$ (py=pyridine) [30, 31], and $\text{Ni}(\text{C}_{10}\text{H}_8\text{N}_2)_2\text{Ni}(\text{CN})_4\cdot\text{H}_2\text{O}$ (NBYC) [32–34].

In this Letter, we fill up the vacancy in the survey of the phase diagram regarding the E -term. By means of the DMRG [35], within the periodic boundary conditions (PBC), the ground-state phase diagram of the $S=1$ Hamiltonian Eq. (1) is shown in the Fig. 1, and some of Q1D spin-1 materials are listed in Tab. I. By the permutations of spin operators, the phase diagram shows a “rotational” symmetry in the rescaled $D-\sqrt{3}E$ parameter space [36]. The Hamiltonian does not conserve the magnetization $M=\sum_i S_i^z$ because of the E -term. Instead of the magnetization, the parity of M is conserved. $m=M \bmod 2=0$ or 1, is a good quantum number since the E -term raises or lowers the magnetization by 2. The spacial inversion and time reversal symmetry are also good quantum numbers $(p, t)=(\pm 1, \pm 1)$ and are considered in the finite-size DMRG algorithm to reduce the dimension of Hilbert space in the diagonalization procedure [14].

Entanglement Spectrum.— With the Haldane gap in the bulk, the ground state in the Haldane phase has free spin-1/2 states at the edges within open boundary conditions. For the PBC, a closed chain in our case, the edge states can be artificially created by the partial trace of one part of the bipartition. Explicitly, the chain is divided into two subsystems A and B with equal sizes, and the reduced density matrix $\rho_A=\text{Tr}_B|\psi_0\rangle\langle\psi_0|$ is computed in the DMRG, where $|\psi_0\rangle$ is the ground state. The entanglement spectrum is defined by $\xi_i=-\ln\omega_i$, where ω_i is the i -th largest eigenvalue of ρ_A [37]. The edge states reflect on that the reduced state can be decomposed into the product $\rho_A \approx (\frac{1}{2}\mathbb{1}_{2 \times 2}) \otimes \rho_0 \otimes (\frac{1}{2}\mathbb{1}_{2 \times 2})$, where $\mathbb{1}_{2 \times 2}$ are the two-by-two identity matrices of the edges, the boundary between A and B, and ρ_0 is a pure-state bulk-part matrix of the subsystem A. This fact ensures a four-

TABLE I. The values of zero-field-splitting parameters for some spin-1 Q1D materials.

Compounds	D/J	E/J	Phase	Ref.
Y_2BaNiO_5	-0.039	-0.0127	Haldane	4
NENB	0.17	-0.016	Haldane	9
NENP	0.2	0.01–0.02	Haldane	8
$[\text{Ni}(\text{HF}_2)(3\text{-Clpy})_4]\text{BF}_4$	0.88	-	-	30,31
NBYC ^a	6.25	2.5	Large- D	32
NBYC ^b	7.49	4.26	Large- D	33
NENC	7.5	0.83	Large- D	29
$\text{Sr}_3\text{NiPtO}_6$	8.8	0	Large- D	27,28

^a Susceptibility.

^b An additional bilinear-biquadratic term is considered.

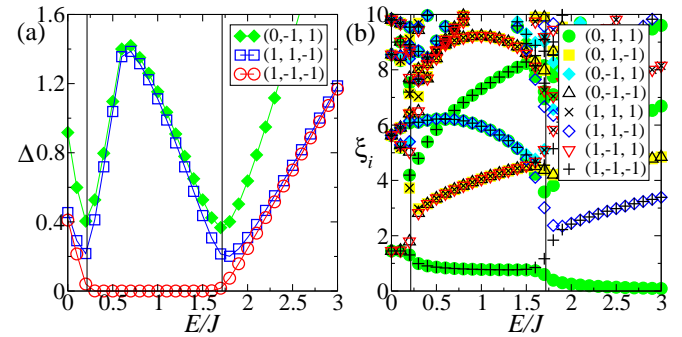


FIG. 2. (a) The excitation gap $\Delta=E_0(m, p, t; \text{PBC})-E_g$, where $E_g=E_0(0, 1, 1; \text{PBC})$ is the ground state energy. The ground state in the y -Néel phase has double degeneracy. (b) The entanglement spectra of at least four-fold, double, and non-degeneracy characterize the Haldane, the y -Néel, and the Large- E_x phases, respectively. The vertical lines indicate two critical points $(E/J)_c \simeq 0.214$ and 1.717 , respectively. DMRG data for $D/J=0$ and $L=80$ are presented.

fold degenerate entanglement spectrum in the Haldane phase [38, 39]. The four-fold degeneracy can be seen as a simple illustration of the bulk-edge correspondence in the entanglement spectrum [40, 41].

Labelled by the quantum numbers (m, p, t) , the lowest energy excitations $\Delta(m, p, t)=E_0(m, p, t; \text{PBC})-E_g$ and the low-lying entanglement spectra are shown in the Fig. 2 for fixed $D/J=0$, where $E_g=E_0(0, 1, 1; \text{PBC})$ is the ground-state energy. The Haldane gap is estimated by $\Delta(1, -1, -1) \simeq 0.41J$ for $D=E=0$, which agrees with previous numerical result [42]. Double degeneracy in the ground-state energy and the entanglement spectrum are found in the region between the Haldane phase and the Large- E_x phase. Both of the double degeneracies come from the nature of a \mathbb{Z}_2 spontaneous symmetry breaking phase, with breaking the parity of magnetization, space inversion, and time-reversal symmetries, simultaneously. The spin-spin correlation shows the phase also breaks translational symmetry, as we will see in Fig. 3, therefore we refer to this phase as the y -Néel phase.

The degeneracy structure of entanglement spectrum has been proposed to distinguish different many-body quantum phases recently [22, 43–45]. The reason of the double degeneracy in the y -Néel phase, Fig. 2(b), is that, the degenerate ground state is selected as an eigenstate of the symmetry operators by the quantum numbers (m, p, t) in the DMRG [14]. Such an enforced symmetrized state is similar to a Greenberger-Horne-Zeilinger (GHZ) state, and the artificial double degenerate spectrum is generated. For example, the state $\frac{1}{\sqrt{2}}(|\diagup\diagup\diagup\rangle \pm |\diagdown\diagdown\diagdown\rangle)$ has the inversion parity quantum number $p=\pm 1$, and it is an entangled state. However, each symmetry breaking state, $|\diagup\diagup\diagup\rangle$ or $|\diagdown\diagdown\diagdown\rangle$, is not an eigenstate of the symmetry operator, and it is not entangled, either. Note that the double degeneracy

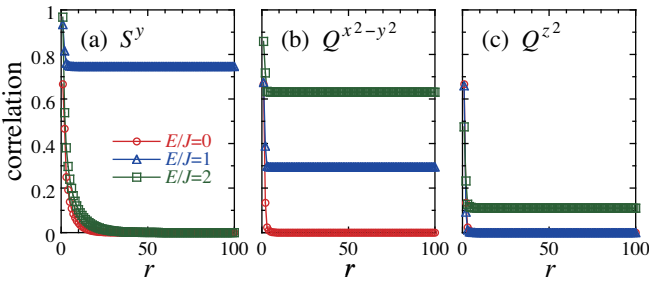


FIG. 3. Spin and quadrupole correlation functions at typical values of E/J for $D/J=0$ and $L=200$. (a) $(-1)^r \langle S_0^y S_r^y \rangle$, (b) $\langle Q_0^{x^2-y^2} Q_r^{x^2-y^2} \rangle$, and (c) $\langle Q_0^{z^2} Q_r^{z^2} \rangle$. Note that $r=100$ for the most distant sites in the periodic chain of $L=200$.

appears in the entire spectrum, and is also found in the z -Néel and x -Néel phases. Thus, the degeneracy structure of the entanglement spectrum identifies the SPT phase (four-fold), the \mathbb{Z}_2 symmetry breaking phase (double), and the topological trivial phase (single).

In the z -Néel phase, the parity of magnetization m is conserved, therefore the other parity quantum numbers (p, t) are essential for observing the degenerate spectrum. In contrast, in the y -Néel (or x -Néel) phase, the double degeneracy can be observed when only using the parity of magnetization. Therefore the E -term serves an ideal model Hamiltonian to observe the parity degeneracy in the spontaneous symmetry breaking phase. From the technical point of view, quantum numbers are usually used in the DMRG for preventing the mixture of different subspace as well as stabilizing and accelerating the computations. Because the magnetization is the most often used quantum number in the DMRG, programming with the parity of magnetization should be easier than the parity of inversion or time-reversal.

Correlation Functions.— The microscopic spin states of novel quantum phases induced by single-ion anisotropies can be clarified by measuring spin correlation functions, $\langle S_0^\alpha S_r^\alpha \rangle$, and quadrupole correlation functions, $\langle Q_0^\gamma Q_r^\gamma \rangle$, where $Q_i^{x^2-y^2} = (S_i^x)^2 - (S_i^y)^2$ and $Q_i^{z^2} = \frac{1}{\sqrt{3}}[3(S_i^z)^2 - 2]$ are relevant quadrupole operators. In Fig. 3, we show typical behavior with increasing E/J for fixed $D/J=0$. In the Haldane phase for small anisotropies, spin and quadrupole correlations are short-ranged, as shown for $E/J=0$. At intermediate E/J , robust antiferromagnetic correlations of the spin y -component occur, as shown for $E/J=1$. Spin correlations of the x - and z -components are short-ranged (not shown). Note here that the local spin state is forced to be the lowest-energy eigenstate of $E[(S_i^x)^2 - (S_i^y)^2]$, given by $|S_i^x=0\rangle$, where the local spin fluctuates in the yz -plane. Such fluctuating spins align antiferromagnetically, while they preferably point to the y -direction due to the E -term. Thus the y -Néel phase is identified. At large E/J , the ground state turns to be the product of $|S_i^x=0\rangle$, and the Néel structure vanishes,

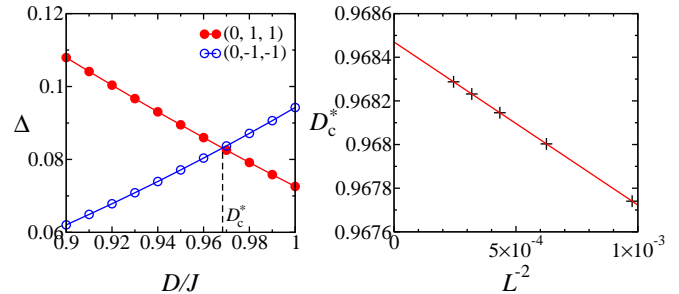


FIG. 4. (Left) Energy level crossing with different quantum numbers occurs at D_c^* for $L=64$, $E/J=0$, within TBC. $\Delta = E_0(m, p, t; \text{TBC}) - E_g$ and $E_g = E_0(0, 1, 1; \text{PBC})$ is the ground state energy within PBC. (Right) Extrapolation of the critical point is performed by linear fitting. $(D/J)_c = 0.9684713(1)$ is obtained.

as shown for $E/J=2$. This phase is referred to as the Large- E_x phase. In addition, a distinct feature is that $|S_i^x=0\rangle$ has quadrupole moments, $\langle Q_i^{x^2-y^2} \rangle = -1$ and $\langle Q_i^{z^2} \rangle = \frac{1}{\sqrt{3}}$, so that finite quadrupole correlations come out. The $Q^{x^2-y^2}$ correlation develops in the y -Néel and Large- E_x phases, while the Q^{z^2} correlation grows after entering the Large- E_x phase. We should note that the E - and D -terms have the same forms as $Q^{x^2-y^2}$ and Q^{z^2} , respectively, indicating emergent quadrupole degrees of freedom. We expect that the competition of quadrupole states would drive the system into quadrupole phases, the so-called spin nematic phases, but Néel phases are observed in the present case at zero magnetic field. The search for possible quadrupole phases in magnetic field would be an interesting future problem, since those in a spin-1/2 frustrated chain in high magnetic field have been actively discussed [46–51].

The critical points are determined by the finite size scaling of the entanglement entropy [36] and the level spectroscopy (LS) method. All the transitions belong to the Ising universality class with the central charge $c=\frac{1}{2}$, except three Gaussian points with $c=1$ labelled by the red points in Fig. 1. Topological quantum phase transitions occur at these Gaussian points, from the Haldane phase to the Large- D , Large- E_x , or Large- E_y phases. The transition from the Haldane phase to the Large- D phase is the third-order Gaussian transition [21], therefore this critical point is more difficult to be precisely determined than the conventional second-order transitions. Several methods for the determination of this critical point were investigated, including the LS plus exact diagonalization (LS+ED) [17], fidelity susceptibility [20, 21], quantum monte carlo (QMC) [52], von Neumann entropy [53] and the quantum renormalization group [54]. Here we use the parity DMRG [14] to perform the LS+DMRG method.

Level Spectroscopy.— The LS method [55–59] is based on the effective field theory of the sine-Gordon model and the $c=1$ conformal field theory. The critical point

can be probed by the energy level crossing within the twisted boundary conditions (TBC), $S_{L+1}^x \rightarrow -S_1^x$, $S_{L+1}^y \rightarrow -S_1^y$, $S_{L+1}^z \rightarrow S_1^z$. We show the energy level crossing $E_0(m, p, t; \text{TBC})$ with different quantum numbers $(m, p, t) = (0, 1, 1)$ and $(0, -1, -1)$ in Fig. 4. The location of the crossing point is labelled by $D/J = D_c^*$, and critical point is obtained by the extrapolation to the thermodynamic limits. It is known that the scaling formula is a polynomial function in L^{-2} [55–59]. This importantly makes the convergence fast, because the subleading term L^{-4} is much smaller than the leading term. Our numerical data [36], for $L = 32, 40, 48, 56$, and 64, show that a linear fitting is good enough for the extrapolation. We obtain $(D/J)_c = 0.96847133(2)$ with linear fitting and $(D/J)_c = 0.96847141(2)$ with the subleading term L^{-4} . Therefore it would be safe to conclude $(D/J)_c = 0.9684713(1)$ with the systematic error about 10^{-7} . Although our LS+DMRG only have sizes $L \leq 64$, combining the DMRG technique proposed by Hu *et al.* for large systems [53] with level spectroscopy should further improve the precision of the value $(D/J)_c$. Other combinations such as LS+QMC [60] are also possible.

Finally, we briefly discuss the effect of E -term at these (red points in Fig. 1) topological critical points. Basically, the effect of E -term can be understood from the scaling dimension of the E -term at the Haldane-Large- D critical point $(D/J)_c$ in the renormalization group flow analysis. If the E -term is relevant at the critical point, the critical point disappears by introducing an infinitesimal E -term as observed in the phase diagram in D - E plane, Fig. 1. The Haldane-Large- D critical point $(D/J)_c$ is characterized by the central charge $c=1$ free boson conformal field theory [18]. Note that the E -term can be transformed as

$$E \sum_{i=1}^L [(S_i^x)^2 - (S_i^y)^2] = \frac{E}{2} \sum_{i=1}^L [(S_i^+)^2 + (S_i^-)^2]. \quad (2)$$

Thus, if the scaling dimension of $(S_i^+)^2$ at the critical fixed point is less than the dimension $1 + 1 = 2$, the E -term is relevant and an infinitesimal E/J flows away from the critical point. The renormalization flow may eventually goes to x - or y -Néel phases depending on the sign of E/J . Actually, a recent DMRG calculation has estimated the scaling dimension Δ_s corresponding to this operator as $\Delta_s = 0.750 \pm 0.002$ [18]. Because the scaling dimension clearly satisfies the relation $\Delta_s < 2$, we can conclude that the effect of E -term is relevant at the Haldane-Large- D critical fixed point $(D/J)_c$. Thus we expect that by introducing infinitesimal E/J , the critical point between the Haldane and the Large- D phases disappears because the relevant E -term increases along renormalization and it flows away from the critical point. By considering the symmetries of permutation of axis [36], the present discussions are also applicable for the critical points between the Haldane phase and Large- E_x or

Large- E_y phases.

Discussions.— We have investigated and provided a precise quantum phase diagram for the $S=1$ Haldane chain with both uniaxial and rhombic single-ion anisotropies, Eq. (1). By the parity DMRG [14] within PBC, we show that, for the first time, the symmetry breaking phase has double degeneracy in the entire entanglement spectrum. This generalizes the perspective that the degeneracy structure of entanglement spectrum tells different quantum phases, from the SPT phases to the symmetry breaking phases. The Haldane-Large- D critical point is determined by the LS+DMRG method with an unprecedented accurate value $(D/J)_c = 0.9684713(1)$. The presented power of the LS+DMRG method supports the reliability of finding the SPT intermediate- D phase in $S=2$ XXZ chain [12–14]. From the phase diagram, we point out that a small rhombic anisotropy induces a transverse antiferromagnetic long range order when D/J close to this $(D/J)_c$. This suggests that $[\text{Ni}(\text{HF}_2)(3\text{-Clpy})_4]\text{BF}_4$, with $D/J \simeq 0.88$ [30], is a possible candidate system to search for the y -Néel phase.

In the end of this Letter, we argue the spin-1 chain can be made by arranging the single-molecule-magnets (SMMs), *e.g.*, CoH, the $S=1$ SMM [61]. We mention that recent experiments on a small cluster of SMMs have been taken into account the weak interactions between SMMs for $L=2$ [62] and $L=4$ [63]. On the other hand, atomic engineering has been able to tune the magnetic anisotropy [64] and tune the spin state by absorbing hydrogen [61, 65]. The spin-spin interaction coming from the superexchange mechanism [66–69] and the Ruderman-Kittel-Kasuya-Yosida (RKKY) interaction [70] have been observed. In principle, an artificial spin chain with both uniaxial and rhombic single-ion anisotropies can be created.

Acknowledgements.— Y.C.T. and Y.J.K. are grateful to MOST in Taiwan via No. MOST105-2112-M-002-023-MY3. H.O. acknowledges the support of JSPS KAKENHI Grant Number JP16K05494. We are grateful to the National Center for High-performance Computing for computer time and facilities. Computations were also done on the supercomputers at the Japan Atomic Energy Agency and the Institute for Solid State Physics, the University of Tokyo. We are grateful to Hui Zhai, Kwai-Kong Ng and Markus Ternes for many useful discussions. T.O. was supported by JSPS KAKENHI Grant Number JP15K17701 and by MEXT of Japan as a social and scientific priority issue (Creation of new functional devices and high-performance materials to support next-generation industries; CDMSI) to be tackled by using post-K computer.

* d102054002@mail.nch.edu.tw

[†] onishi.hiroaki@jaea.go.jp

[‡] yjkao@phys.ntu.edu.tw

[1] F. D. M. Haldane, “Nonlinear field theory of large-spin Heisenberg antiferromagnets: Semiclassically quantized solitons of the one-dimensional easy-axis Néel state,” *Phys. Rev. Lett.* **50**, 1153–1156 (1983).

[2] W. J. L. Buyers, R. M. Morra, R. L. Armstrong, M. J. Hogan, P. Gerlach, and K. Hirakawa, “Experimental evidence for the Haldane gap in a spin-1 nearly isotropic, antiferromagnetic chain,” *Phys. Rev. Lett.* **56**, 371–374 (1986).

[3] M. Kenzelmann, R. A. Cowley, W. J. L. Buyers, Z. Tun, R. Coldea, and M. Enderle, “Properties of Haldane excitations and multiparticle states in the antiferromagnetic spin-1 chain compound CsNiCl_3 ,” *Phys. Rev. B* **66**, 024407 (2002).

[4] Guangyong Xu, J. F. DiTusa, T. Ito, K. Oka, H. Takagi, C. Broholm, and G. Aeppli, “ Y_2BaNiO_5 : A nearly ideal realization of the $S=1$ Heisenberg chain with antiferromagnetic interactions,” *Phys. Rev. B* **54**, R6827–R6830 (1996).

[5] C. Rudowicz, P. Gnutek, S. Kimura, M. Açıkgöz, and Y. Y. Yeung, “Modeling spectroscopic properties of Ni^{2+} ions in the Haldane gap system Y_2BaNiO_5 ,” *Applied Magnetic Resonance* **44**, 899–915 (2013).

[6] P. Gnutek, M. Açıkgöz, and C. Rudowicz, “Tools for magnetostructural correlations for the $3d^8(^3\text{A}_2$ state) ions at orthorhombic sites: Comparative study with applications to Ni^{2+} ions in Y_2BaNiO_5 and $\text{Nd}_2\text{BaNiO}_5$,” *J. Mag. Mag. Mat.* **374**, 484 – 494 (2015).

[7] J. P. Renard, M. Verdaguer, L. P. Regnault, W. A. C. Erkelens, J. Rossat-Mignod, and W. G. Stirling, “Presumption for a quantum energy gap in the quasi-one-dimensional $S=1$ Heisenberg antiferromagnet $\text{Ni}(\text{C}_2\text{H}_8\text{N}_2)_2\text{NO}_2(\text{ClO}_4)$,” *EPL (Europhysics Letters)* **3**, 945 (1987).

[8] L. P. Regnault and J. P. Renard, “Spin dynamics in the Haldane-gap system NENP,” *Physica B* **215**, 71–76 (1995).

[9] E. Čižmár, M. Ozerov, O. Ignatchik, T. P. Papanagorgiou, J. Wosnitza, S. A. Zvyagin, J. Krzystek, Z. Zhou, C. P. Landee, B. R. Landry, M. M. Turnbull, and J. L. Wikaira, “Magnetic properties of the Haldane-gap material $[\text{Ni}(\text{C}_2\text{H}_8\text{N}_2)_2\text{NO}_2](\text{BF}_4)$,” *New J. Phys.* **10**, 033008 (2008).

[10] Zheng-Cheng Gu and Xiao-Gang Wen, “Tensor-entanglement-filtering renormalization approach and symmetry-protected topological order,” *Phys. Rev. B* **80**, 155131 (2009).

[11] Frank Pollmann, Erez Berg, Ari M. Turner, and Masaki Oshikawa, “Symmetry protection of topological phases in one-dimensional quantum spin systems,” *Phys. Rev. B* **85**, 075125 (2012).

[12] Takashi Tonegawa, Kiyomi Okamoto, Hiroki Nakano, Tōru Sakai, Kiyohide Nomura, and Makoto Kaburagi, “Haldane, large- D , and intermediate- D states in an $S=2$ quantum spin chain with on-site and XXZ anisotropies,” *J. Phys. Soc. Jpn.* **80**, 043001 (2011).

[13] Kiyomi Okamoto, Takashi Tonegawa, and Tōru Sakai, “Ground-state phase diagram of the bond-alternating $S=2$ quantum spin chain with the XXZ and on-site anisotropies – symmetry protected topological phase versus trivial phase –,” *J. Phys. Soc. Jpn.* **85**, 063704 (2016).

[14] Yu-Chin Tzeng, “Parity quantum numbers in the density matrix renormalization group,” *Phys. Rev. B* **86**, 024403 (2012).

[15] Jonas A. Kjäll, Michael P. Zaletel, Roger S. K. Mong, Jens H. Bardarson, and Frank Pollmann, “Phase diagram of the anisotropic spin-2 XXZ model: Infinite-system density matrix renormalization group study,” *Phys. Rev. B* **87**, 235106 (2013).

[16] Ian Affleck, Tom Kennedy, Elliott H. Lieb, and Hal Tasaki, “Rigorous results on valence-bond ground states in antiferromagnets,” *Phys. Rev. Lett.* **59**, 799–802 (1987).

[17] Wei Chen, Kazuo Hida, and B. C. Sanctuary, “Ground-state phase diagram of $S=1$ XXZ chains with uniaxial single-ion-type anisotropy,” *Phys. Rev. B* **67**, 104401 (2003).

[18] C. Degli Esposti Boschi, E. Ercolessi, F. Ortolani, and M. Roncaglia, “On $c=1$ critical phases in anisotropic spin-1 chains,” *Eur. Phys. J. B* **35**, 465–473 (2003).

[19] L. Campos Venuti, C. Degli Esposti Boschi, E. Ercolessi, G. Morandi, F. Ortolani, S. Pasini, and M. Roncaglia, “Stable particles in anisotropic spin-1 chains,” *Eur. Phys. J. B* **53**, 11–18 (2006).

[20] Yu-Chin Tzeng and Min-Fong Yang, “Scaling properties of fidelity in the spin-1 anisotropic model,” *Phys. Rev. A* **77**, 012311 (2008).

[21] Yu-Chin Tzeng, Hsiang-Hsuan Hung, Yung-Chung Chen, and Min-Fong Yang, “Fidelity approach to Gaussian transitions,” *Phys. Rev. A* **77**, 062321 (2008).

[22] Frank Pollmann, Ari M. Turner, Erez Berg, and Masaki Oshikawa, “Entanglement spectrum of a topological phase in one dimension,” *Phys. Rev. B* **81**, 064439 (2010).

[23] Yousef Rahnavard and Wolfram Brenig, “Spin dynamics of the anisotropic spin-1 antiferromagnetic chain at finite magnetic fields,” *Phys. Rev. B* **91**, 054405 (2015).

[24] Yohei Fuji, “Effective field theory for one-dimensional valence-bond-solid phases and their symmetry protection,” *Phys. Rev. B* **93**, 104425 (2016).

[25] Makoto Kaburagi and Takashi Tonegawa, “Effects of the single-ion-type anisotropy on the spin-1 Haldane system with a spin-1/2 impurity,” *Physica B* **211**, 193 – 195 (1995).

[26] Czesław Rudowicz, “Effect of small in-plane anisotropy in the large- D phase systems based on Ni^{2+} ($S=1$) ions in Heisenberg antiferromagnetic chains,” *Physica B* **436**, 193 (2014).

[27] S. Chattopadhyay, Deepti Jain, V. Ganesan, S. Giri, and S. Majumdar, “Observation of large- D magnetic phase in $\text{Sr}_3\text{NiPtO}_6$,” *Phys. Rev. B* **82**, 094431 (2010).

[28] A.-M. Pradipto, R. Broer, and S. Picozzi, “Ab initio modelling of magnetic anisotropy in $\text{Sr}_3\text{NiPtO}_6$,” *Phys. Chem. Chem. Phys.* **18**, 4078–4085 (2016).

[29] M. Orendáč, A. Orendáčová, J. Černák, A. Feher, P. J. C. Signore, M. W. Meisel, S. Merah, and M. Verdaguer, “Thermodynamic and magnetic properties of the $S=1$ Heisenberg chain $\text{Ni}(\text{C}_2\text{H}_8\text{N}_2)_2\text{Ni}(\text{CN})_4$: Experiments and theory,” *Phys. Rev. B* **52**, 3435–3440 (1995).

[30] Jamie L. Manson, Adora G. Baldwin, Brian L. Scott, Jesper Bendix, Rico E. Del Sesto, Paul A. Goddard, Yoshimitsu Kohama, Hope E. Tran, Saman Ghannadzadeh, John Singleton, Tom Lancaster, Johannes S. Möller, Stephen J. Blundell, Francis L. Pratt, Vivien S. Zapf, Jinhee Kang, Changhoon

Lee, Myung-Hwan Whangbo, and Christopher Baines, “[Ni(HF₂)(3-Clpy)₄]BF₄ (py=pyridine): Evidence for spin exchange along strongly distorted F...H...F⁻ bridges in a one-dimensional polymeric chain,” *Inorg. Chem.* **51**, 7520–7528 (2012).

[31] Jian-Sheng Xia, Andrzej Ozarowski, Peter M. Spurgeon, Adora G. Baldwin, Jamie L. Manson, and Mark W. Meisel, “Unusual magnetic response of an *S*=1 antiferromagnetic linear-chain material,” [arXiv:1409.5971](https://arxiv.org/abs/1409.5971) (2014).

[32] M. Orendáč, E. Čižmár, A. Orendáčová, J Černák, A. Feher, M. W. Meisel, K. A. Abboud, S. Zvyagin, M. Sieling, T. Rieth, and B. Lüthi, “Magnetic and thermodynamic properties of Ni(C₁₀H₈N₂)₂Ni(CN)₄·H₂O: A *S*=1 Heisenberg antiferromagnetic chain with strong in-plane anisotropy and subcritical exchange coupling,” *Phys. Rev. B* **61**, 3223–3226 (2000).

[33] M. T. Batchelor, Xi-Wen Guan, and Norman Oelkers, “Thermal and magnetic properties of spin-1 magnetic chain compounds with large single-ion and in-plane anisotropies,” *Phys. Rev. B* **70**, 184408 (2004).

[34] M. T. Batchelor, X.-W. Guan, N. Oelkers, and A. Foerster, “Thermal and magnetic properties of integrable spin-1 and spin-3/2 chains with applications to real compounds,” *J. Stat. Mech.: Theor. Exp.* **2004**, P10017 (2004).

[35] Steven R. White, “Density matrix formulation for quantum renormalization groups,” *Phys. Rev. Lett.* **69**, 2863–2866 (1992).

[36] Please see the supplementary materials.

[37] Hui Li and F. D. M. Haldane, “Entanglement spectrum as a generalization of entanglement entropy: Identification of topological order in non-abelian fractional quantum Hall effect states,” *Phys. Rev. Lett.* **101**, 010504 (2008).

[38] Yu-Chin Tzeng, Li Dai, M.-C. Chung, Luigi Amico, and Leong-Chuan Kwek, “Entanglement convertibility by sweeping through the quantum phases of the alternating bonds XXZ chain,” *Sci. Rep.* **6**, 26453 (2016).

[39] Hannes Pichler, Guanyu Zhu, Alireza Seif, Peter Zoller, and Mohammad Hafezi, “Measurement protocol for the entanglement spectrum of cold atoms,” *Phys. Rev. X* **6**, 041033 (2016).

[40] Anushya Chandran, M. Hermanns, N. Regnault, and B. A. Bernevig, “Bulk-edge correspondence in entanglement spectra,” *Phys. Rev. B* **84**, 205136 (2011).

[41] Xiao-Liang Qi, Hoshio Katsura, and Andreas W. W. Ludwig, “General relationship between the entanglement spectrum and the edge state spectrum of topological quantum states,” *Phys. Rev. Lett.* **108**, 196402 (2012).

[42] Satoshi Ejima and Holger Fehske, “Comparative density-matrix renormalization group study of symmetry-protected topological phases in spin-1 chain and Bose-Hubbard models,” *Phys. Rev. B* **91**, 045121 (2015).

[43] Wei Li, Andreas Weichselbaum, and Jan von Delft, “Identifying symmetry-protected topological order by entanglement entropy,” *Phys. Rev. B* **88**, 245121 (2013).

[44] Sukhwinder Singh, “Identifying quantum phases from the injectivity of symmetric matrix product states,” *Phys. Rev. B* **91**, 115145 (2015).

[45] S. N. Saadatmand and I. P. McCulloch, “Symmetry fractionalization in the topological phase of the spin- $\frac{1}{2}$ J_1-J_2 triangular Heisenberg model,” *Phys. Rev. B* **94**, 121111 (2016), arXiv:1704.03418 (2017).

[46] Andrey V. Chubukov, “Chiral, nematic, and dimer states in quantum spin chains,” *Phys. Rev. B* **44**, 4693(R) (1991).

[47] Toshiya Hikihara, Lars Kecke, Tsutomu Momoi, and Akira Furusaki, “Vector chiral and multipolar orders in the spin-1/2 frustrated ferromagnetic chain in magnetic field,” *Phys. Rev. B* **78**, 144404 (2008).

[48] Hiroaki Onishi, “Magnetic excitations of spin nematic state in frustrated ferromagnetic chain,” *J. Phys. Soc. Jpn.* **84**, 083702 (2015).

[49] Hiroaki Onishi, “Effects of magnetic anisotropy on spin dynamics of ferromagnetic frustrated chain,” *J. Phys.: Conf. Ser.* **592**, 012109 (2015).

[50] Takatsugu Masuda, Masato Hagihara, Yusuke Kondoh, Koji Kaneko, and Naoto Metoki, “Spin density wave in insulating ferromagnetic frustrated chain LiCuVO₄,” *J. Phys. Soc. Jpn.* **80**, 113705 (2011).

[51] M. Mourigal, M. Enderle, B. Fåk, R. K. Kremer, J. M. Law, A. Schneidewind, A. Hiess, and A. Prokofiev, “Evidence of a bond-nematic phase in LiCuVO₄,” *Phys. Rev. Lett.* **109**, 027203 (2012).

[52] A. F. Albuquerque, C. J. Hamer, and J. Oitmaa, “Quantum phase diagram and excitations for the one-dimensional *S*=1 Heisenberg antiferromagnet with single-ion anisotropy,” *Phys. Rev. B* **79**, 054412 (2009).

[53] Shijie Hu, B. Normand, Xiaoqun Wang, and Lu Yu, “Accurate determination of the Gaussian transition in spin-1 chains with single-ion anisotropy,” *Phys. Rev. B* **84**, 220402 (2011).

[54] A. Langari, F. Pollmann, and M. Siahatgar, “Ground-state fidelity of the spin-1 Heisenberg chain with single ion anisotropy: quantum renormalization group and exact diagonalization approaches,” *J. Phys.: Cond. Matt.* **25**, 406002 (2013).

[55] K. Nomura, “Correlation functions of the 2D sine-Gordon model,” *J. Phys. A: Math. Gen.* **28**, 5451 (1995).

[56] A. Kitazawa, “Twisted boundary conditions of quantum spin chains near the Gaussian fixed points,” *Phys. A: Math. Gen.* **30**, L285 (1997).

[57] Atsuhiro Kitazawa and Kiyohide Nomura, “Critical properties of *S*=1 bond-alternating XXZ chains and hidden $Z_2 \times Z_2$ symmetry,” *J. Phys. Soc. Jpn.* **66**, 3944–3956 (1997).

[58] Atsuhiro Kitazawa and Kiyohide Nomura, “Phase transitions of *S*=3/2 and *S*=2 XXZ spin chains with bond alternation,” *J. Phys. Soc. Jpn.* **66**, 3379–3382 (1997).

[59] Kiyohide Nomura and Atsuhiro Kitazawa, “SU(2)/Z₂ symmetry of the BKT transition and twisted boundary condition,” *J. Phys. A: Math. Gen.* **31**, 7341 (1998).

[60] Hidemaro Suwa and Synge Todo, “Generalized moment method for gap estimation and quantum monte carlo level spectroscopy,” *Phys. Rev. Lett.* **115**, 080601 (2015).

[61] Peter Jacobson, Tobias Herden, Matthias Muenks, Gennadii Laskin, Oleg Brovko, Valeri Stepanyuk, Markus Ternes, and Klaus Kern, “Quantum engineering of spin and anisotropy in magnetic molecular junctions,” *Nat. Commun.* **6**, 8536 (2015).

[62] Wolfgang Wernsdorfer, Núria Aliaga-Alcalde, David N. Hendrickson, and George Christou, “Exchange-biased quantum tunnelling in a supramolecular dimer of single-molecule magnets,” *Nature* **416**, 406–409 (2002).

[63] Tu N. Nguyen, Wolfgang Wernsdorfer, Muhandis Shiddiq, Khalil A. Abboud, Stephen Hill, and

George Christou, "Supramolecular aggregates of single-molecule magnets: exchange-biased quantum tunneling of magnetization in a rectangular $[\text{Mn}_3]_4$ tetramer," *Chem. Sci.* **7**, 1156–1173 (2016).

[64] A. A. Khajetoorians, M. Valentyuk, *et al.*, "Tuning emergent magnetism in a Hund's impurity," *Nature nanotechnology* **10**, 958–964 (2015).

[65] Liwei Liu, Kai Yang, *et al.*, "Reversible single spin control of individual magnetic molecule by hydrogen atom adsorption," *Sci. Rep.* **3**, 1210 (2013).

[66] Cyrus F. Hirjibehedin, Christopher P. Lutz, and Andreas J. Heinrich, "Spin coupling in engineered atomic structures," *Science* **312**, 1021–1024 (2006).

[67] Chiung-Yuan Lin and B. A. Jones, "First-principles calculations of engineered surface spin structures," *Phys. Rev. B* **83**, 014413 (2011).

[68] A. F. Otte, M. Ternes, S. Loth, C. P. Lutz, C. F. Hirjibehedin, and A. J. Heinrich, "Spin excitations of a kondo-screened atom coupled to a second magnetic atom," *Phys. Rev. Lett.* **103**, 107203 (2009).

[69] Sebastian Loth, Susanne Baumann, Christopher P. Lutz, D. M. Eigler, and Andreas J. Heinrich, "Bistability in atomic-scale antiferromagnets," *Science* **335**, 196–199 (2012).

[70] A. A. Khajetoorians, M. Steinbrecher, M. Ternes, *et al.*, "Tailoring the chiral magnetic interaction between two individual atoms," *Nat. Commun.* **7**, 10620 (2016).

[71] Luigi Amico, Rosario Fazio, Andreas Osterloh, and Vlatko Vedral, "Entanglement in many-body systems," *Rev. Mod. Phys.* **80**, 517–576 (2008).

[72] G. Vidal, J. I. Latorre, E. Rico, and A. Kitaev, "Entanglement in quantum critical phenomena," *Phys. Rev. Lett.* **90**, 227902 (2003).

[73] V. E. Korepin, "Universality of entropy scaling in one dimensional gapless models," *Phys. Rev. Lett.* **92**, 096402 (2004).

[74] Pasquale Calabrese, Massimo Campostrini, Fabian Essler, and Bernard Nienhuis, "Parity effects in the scaling of block entanglement in gapless spin chains," *Phys. Rev. Lett.* **104**, 095701 (2010).

SUPPLEMENTARY MATERIALS: QUANTUM PHASE TRANSITIONS DRIVEN BY RHOMBIC-TYPE SINGLE-ION ANISOTROPY IN THE $S=1$ HALDANE CHAIN

Yu-Chin Tzeng^{1,2}, Hiroaki Onishi³, Tsuyoshi Okubo⁴, Ying-Jer Kao^{2,5}

¹*Department of Physics, National Chung-Hsing University, Taichung 40227, Taiwan*

²*Department of Physics, National Taiwan University, Taipei 10617, Taiwan*

³*Advanced Science Research Center, Japan Atomic Energy Agency, Tokai, Ibaraki 319-1195, Japan*

⁴*Department of Physics, University of Tokyo, Tokyo 113-0033, Japan*

⁵*National Center of Theoretical Sciences, National Tsing Hua University, Hsinchu 300, Taiwan*

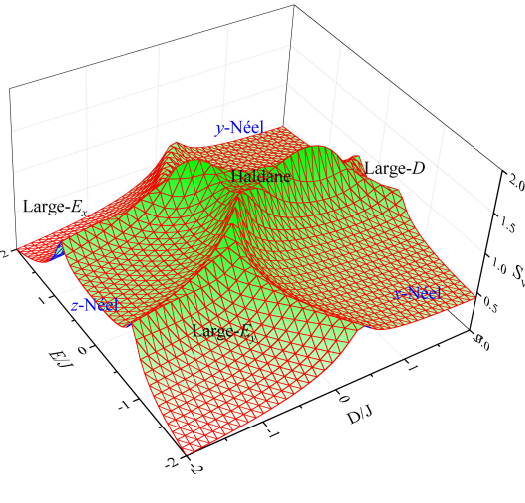


FIG. 5. The von Neumann entropy in the parameter space for $L = 40$. The subsystem size is $L_A = L/2$. The entropy diverges at the critical points in the thermodynamic limits, and remains a finite peaks in the finite size.

Entanglement entropy

The entanglement in many-body systems has been developing as tools and perspective to the quantum critical phenomena [71]. The entanglement entropy is designed for quantifying the entanglement between A and B. The Rényi entropies $S_\alpha = \frac{1}{1-\alpha} \ln(\sum_i \omega_i^\alpha)$ and the von Neumann entropy $S_v = -\sum_i \omega_i \ln \omega_i$ are two common used entropies, and it is convenient to be calculated in the DMRG. It was shown that these entropies diverge logarithmically with the subsystem size L_A at the gapless quantum critical points, $S_v \propto \frac{c}{3} \log L_A$, where c is the central charge in the conformal field theory [72–74]. In principle, the Rényi entropies and the lowest entanglement spectrum ξ_0 are also able to obtain the same critical points [38]; however, here we only perform the finite size scaling on the von Neumann entropy with the subsystem size $L_A = L/2$. The von Neumann entropy for $L = 40$ in the D - E parameter space is shown in Fig. 5, and it is clear that the von Neumann entropy has a peak at the critical point. We label the value and the location of the peak

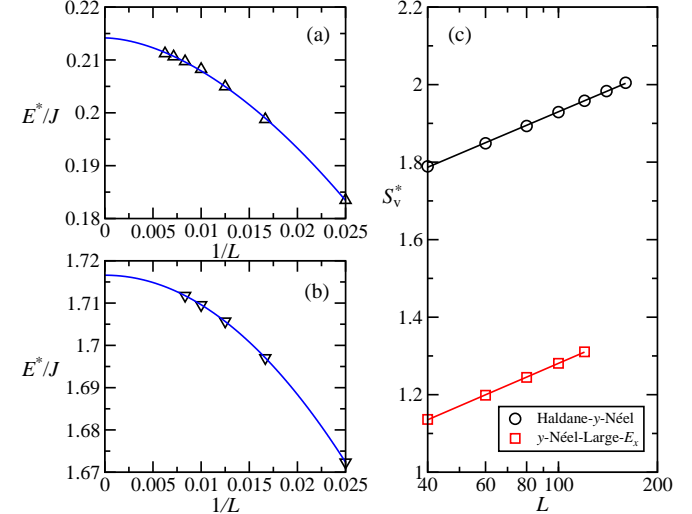


FIG. 6. Finite size scaling of the von Neumann entropy for fixed $D = 0$. (a) The Haldane- y -Néel critical point is about $(E/J)_c \simeq 0.214$. (b) The y -Néel-Large- E_x critical point is about $(E/J)_c \simeq 1.717$. (c) The central charges are obtained by $c \simeq 0.469$ and $c \simeq 0.477$ for Haldane- y -Néel and y -Néel-Large- E_x transitions, respectively.

as S_v^* and E^*/J (or D^*/J for fixed E/J) for fixed D/J , respectively. As shown in Fig. 6, after the finite size scaling, the critical points for fixed $D/J = 0$ are obtained by $(E/J)_c \simeq 0.214$ and $(E/J)_c \simeq 1.717$. The corresponding central charge are $c \simeq 0.469$ and $c \simeq 0.477$, respectively, and this indicates both the transitions belong to the Ising universality class. We obtain the central charge $c \approx \frac{1}{2}$ for all the critical points except three points, which are labeled by the red points in the phase diagram Fig. 1(a). It is known that the transition from the Haldane phase to the Large- D phase is a Gaussian transition with the central charge $c = 1$ [18, 19]. It is suitable to locate this critical point by the level spectroscopy method.

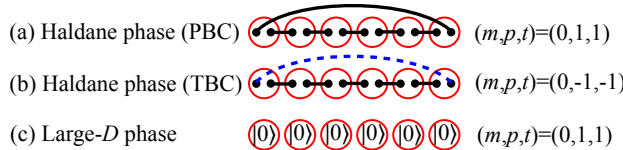


FIG. 7. The VBS picture for the Haldane phase within PBC and TBC are shown in (a) and (b), respectively. The circle represents a spin-1 site, and the dot represents a spin-1/2. The line connecting two spin-1/2 represents a valence bond, the singlet state $\frac{1}{\sqrt{2}}(|\uparrow\downarrow\rangle - |\downarrow\uparrow\rangle)$. The dashed line represents the triplet state within TBC. For the system with even number of the spin-1, the quantum numbers of the ground states in the Handalen phase are $(m, p, t) = (0, 1, 1)$ and $(0, -1, -1)$ within the PBC and TBC, respectively. On the other hand, for both PBC and TBC, the quantum numbers are $(m, p, t) = (0, 1, 1)$ in the Large- D phase, as shown in (c).

Level spectroscopy for the Haldane-Large- D critical point

The continuous quantum phase transitions are possible detected by the level crossing of excited states. The LS has been performed by different numerical algorithm with large system sizes, *e.g.*, LS+DMRG [14] and LS+QMC [60]. The topological quantum phase transition from the Haldane phase to the Large- D phase is known as an example of the third-order Gaussian transition [21], therefore this critical point is more difficult to be precisely determined than the conventional second-order transitions. The LS method [55–59] is based on the effective field theory of the sine-Gordon model and the $c=1$ conformal field theory. Another unrigorous reason of why the method works can be described by the Valence-Bond-Solid (VBS) picture. It was proposed by Affleck, Kennedy, Lieb, and Tasaki (AKLT) that the VBS picture describes the ground state of the Haldane phase [16]. Each spin-1 in the chain is regarded as triplet states of two spin-1/2, and the neighbouring spin-1/2 of different spin-1 form a valence bond, the singlet state $\frac{1}{\sqrt{2}}(|\uparrow\downarrow\rangle - |\downarrow\uparrow\rangle)$, as shown in Fig. 7. This is the exact ground state for the $S = 1$ AKLT model [16], $H = \sum_i \vec{S}_i \cdot \vec{S}_{i+1} + \frac{1}{3} \sum_i (\vec{S}_i \cdot \vec{S}_{i+1})^2$. With replacing the $\frac{1}{3}$ by a tuning parameter β in the bilinear-biquadratic term, the ground state is adiabatically connected from the AKLT model, $\beta = \frac{1}{3}$, to the Heisenberg model, $\beta = 0$, continuously. Thus, the ground states in the Haldane phase share the same VBS picture. On the other hand, the ground states in the Large- D phase are understood by the nearly product state $\prod_i |S_i^z = 0\rangle$. Therefore, by introducing the twisted boundary conditions (TBC), $S_{L+1}^x \rightarrow -S_1^x$, $S_{L+1}^y \rightarrow -S_1^y$, $S_{L+1}^z \rightarrow S_1^z$, the lowest energy states in the Haldane phase and the Large- D phase have different quantum numbers (m, p, t) .

For the system with even number of the spin-1, there are odd number of singlet bonds and one triplet bond in

TABLE II. We show the data for the location of the level crossing D_c^* with different finite sizes. K is the number of state kept in the DMRG.

L	D_c^*	K	truncation errors
32	0.96774204157	1500	1.1×10^{-10}
40	0.96800455535	1500	2.5×10^{-10}
48	0.96814719145	1500	3.7×10^{-10}
56	0.96823319962	2000	2.3×10^{-10}
64	0.96828901845	2000	4.8×10^{-10}
∞	0.96847133(2) ^a		
∞	0.96847141(2) ^b		

^a linear fitting

^b parabolic fitting

the Haldane phase within TBC. Each singlet bond contributes the inversion parity quantum number $p_i = -1$, and the triplet bond contributes $p_L = 1$. Thus, the quantum number for the system becomes odd, $p = \prod_{i=1}^L p_i = -1$. On the other hand, the inversion parity quantum number for the Large- D phase is always even, $p = 1$. Therefore, the Haldane phase and the Large- D phase are characterized by the energy $E_0(0, -1, -1; \text{TBC})$ and $E_0(0, 1, 1; \text{TBC})$, respectively. Here, we list the numerical data in the Tab. II. Up to 2000 states are kept in the DMRG, and the largest truncation error is about 4.8×10^{-10} . The errors in the Lanczos algorithm for the ground state energies are smaller than 10^{-13} , and the dimension of the (m, p, t) -subspace for the Lanczos diagonalization is about 4×10^7 . Four sweeps are performed.

Symmetry of parameters in Heisenberg models with the single-ion anisotropies

In this section, we will discuss the symmetries of parameters in the Hamiltonian given by

$$H = J \sum_{\langle i,j \rangle} \vec{S}_i \cdot \vec{S}_j + D \sum_i (S_i^z)^2 + E \sum_i [(S_i^x)^2 - (S_i^y)^2]. \quad (3)$$

First, we can easily see that the model has a symmetry with respect to the sign flip of E because the sign of E can be absorbed into the exchange of S^x and S^y . In addition to this symmetry, the Hamiltonian has a symmetry with respect to the permutation of spin operators. Note that the Heisenberg interaction is unchanging with respect to the permutation of S^x , S^y and S^z operators. Thus, the ground states of the model share qualitatively same properties among the models obtained by permuting the S^x , S^y , and S^z terms in the single-ion anisotropy terms: such new models are

$$H' = J \sum_{\langle i,j \rangle} \vec{S}_i \cdot \vec{S}_j + D \sum_i (S_i^x)^2 + E \sum_i [(S_i^y)^2 - (S_i^z)^2], \quad (4)$$

and

$$H'' = J \sum_{\langle i,j \rangle} \vec{S}_i \cdot \vec{S}_j + D \sum_i (S_i^y)^2 + E \sum_i [(S_i^z)^2 - (S_i^x)^2]. \quad (5)$$

Because of this permutation symmetry, the ground-state phase diagram of the model has the symmetry in the parameter space spanned by D and E . In the following, we investigate the symmetry in the phase diagram.

In order to investigate the permutation symmetry, here we focus on the single-ion anisotropy terms and consider the one body Hamiltonian

$$H_{\text{SA}} = DS_z^2 + E(S_x^2 - S_y^2). \quad (6)$$

By using the identity relation

$$S^2 = S_x^2 + S_y^2 + S_z^2, \quad (7)$$

we can remove one of the spin operators (S_x , S_y or S_z) from the Hamiltonian. Thus, we have three representations of the Hamiltonian as

$$H_{\text{SA}} = (E - D)S_x^2 - (E + D)S_y^2 + DS_z^2, \quad (8)$$

$$H_{\text{SA}} = -2ES_y^2 - (E - D)S_z^2 + ES_x^2, \quad (9)$$

and

$$H_{\text{SA}} = (D + E)S_z^2 + 2ES_x^2 - ES^2. \quad (10)$$

Note that the terms proportional to S^2 is constant and it does not change the ground state. Thus, hereafter, we neglect these constant terms for the simplicity.

From these three representations, we can easily see that the model with $E = 0$ ($H_{\text{SA}} = DS_z^2$) corresponds to the models with $E = D$ ($H_{\text{SA}} = -2ES_y^2$) and $E = -D$ ($H_{\text{SA}} = 2ES_x^2$). Thus, the topological phase transition between the Haldane phase and the Large- D phase at D_c is mapped on two points $(D, E) = (\frac{1}{2}D_c, \pm\frac{1}{2}D_c)$.

In addition to this mapping, we can see a “rotational” symmetry by introducing a rescaled parameter

$\tilde{E} = \sqrt{3}E$. In order to see the rotational symmetry, we introduce the polar coordinate in the parameter space (D, \tilde{E}) as

$$(D, \tilde{E}) = r(\cos \theta, \sin \theta). \quad (11)$$

By substituting this relation into Eq. (8), we obtain

$$H_{\text{SA}} = \frac{2r}{\sqrt{3}} \left[\sin(\theta - \frac{\pi}{3})S_x^2 - \sin(\theta + \frac{\pi}{3})S_y^2 \right]. \quad (12)$$

In the same way, we transform Eqs. (9) and (10) as

$$H_{\text{SA}} = \frac{2r}{\sqrt{3}} \left[-\sin(\theta)S_y^2 - \sin(\theta - \frac{\pi}{3})S_z^2 \right], \quad (13)$$

and

$$H_{\text{SA}} = \frac{2r}{\sqrt{3}} \left[\sin(\theta + \frac{\pi}{3})S_z^2 + \sin(\theta)S_x^2 \right], \quad (14)$$

respectively. Now, we can see the rotational symmetry easily. If we rotate the parameter by 120 degrees as $\theta \rightarrow \theta + \frac{2\pi}{3}$, Eq. (12) becomes

$$H_{\text{SA}} = \frac{2r}{\sqrt{3}} \left[\sin(\theta + \frac{\pi}{3})S_x^2 + \sin(\theta)S_y^2 \right]. \quad (15)$$

This is equivalent to Eq. (14) by permuting spin operators as $S_x \rightarrow S_z$, $S_y \rightarrow S_x$ and $S_z \rightarrow S_y$. In the same way, by -120 degrees rotation, $\theta \rightarrow \theta - \frac{2\pi}{3}$, we obtain

$$H_{\text{SA}} = \frac{2r}{\sqrt{3}} \left[-\sin(\theta)S_x^2 - \sin(\theta - \frac{\pi}{3})S_y^2 \right]. \quad (16)$$

This is equivalent to Eq. (13) by permuting spin operators as $S_x \rightarrow S_y$, $S_y \rightarrow S_z$ and $S_z \rightarrow S_x$.

As we emphasized previously, the Heisenberg coupling is unchanging under such permutations of spin operators. Thus, when we consider the phase diagram of the model Eq. (3) in (D, \tilde{E}) plane, the phase boundaries must have the symmetry with respect to 120 degrees rotation. We can also map the characteristics of each phase by considering the permutations of spin operators.